

GMSS2.0: An Enhanced Software Program for Stochastic Finite-Fault Ground-Motion Simulation

Yuxiang Tang^{*1,2} 

Abstract

This article introduces an enhanced software program for stochastic ground-motion simulations using finite-fault sources, named Ground-Motion Simulation System version 2.0 (GMSS2.0). GMSS2.0 embodies an updated theoretical model of corner frequency and source duration, making the seismological model for defining the Fourier amplitude spectrum for each subfault more theoretically consistent. In addition, GMSS2.0 provides four rupture scaling relationships and five baseline correction techniques for end users to select the most suitable one for a specific application. For validation purposes, comprehensive comparisons between GMSS2.0 and EXtended SIMulation (EXSIM) for wide ranges of magnitude (M 4–8), distance (~ 6 –300 km) and spectral period (0.01–10 s) have been performed. The results show that GMSS2.0 can give remarkably close estimates to EXSIM with reasonable levels of accuracy. Finally, further validation is performed by comparing GMSS2.0 simulations with five Next Generation Attenuation-West2 ground-motion models for multiple scenario earthquakes with the updated site amplification for the generic California condition ($V_{530} = 500$ m/s).

Cite this article as Tang, Y. (2022). GMSS2.0: An Enhanced Software Program for Stochastic Finite-Fault Ground-Motion Simulation, *Seismol. Res. Lett.* **XX**, 1–12, doi: [10.1785/0220210228](https://doi.org/10.1785/0220210228).


Introduction

Stochastic ground-motion simulation is an important and reliable approach for generating synthetic accelerograms for engineering interests, even though there is an increasing trend of using the broadband ground-motion simulation method (Boore, 2009). Stochastic ground-motion simulation based on finite-fault sources, compared with point sources, is more prudent for considering the source geometric characteristics and wave propagation directivity features (Beresnev and Atkinson, 1998a). Therefore, the stochastic finite-fault ground-motion simulation approach has been widely utilized during the past decades. For example, Atkinson and Boore (2006) used the stochastic finite-fault simulation approach to develop a ground-motion model (GMM, also known as ground-motion prediction equation) for eastern North America (ENA), and this model is widely used for representing the ground-motion levels for Eastern North America (ENA) and ENA-proxy conditions. Allen (2012) employed this approach to develop a GMM for southeastern Australia (SEA), and this GMM was incorporated in the national seismic-hazard analysis program to quantify the hazard level at SEA (Allen *et al.*, 2018).

FINSIM is an algorithm for implementing stochastic finite-fault ground-motion simulation (Beresnev and Atkinson, 1998b). The basic idea of FINSIM is to divide the earthquake fault into several subfaults and treat each subfault as a point source. The total ground motion is the summation of the ground

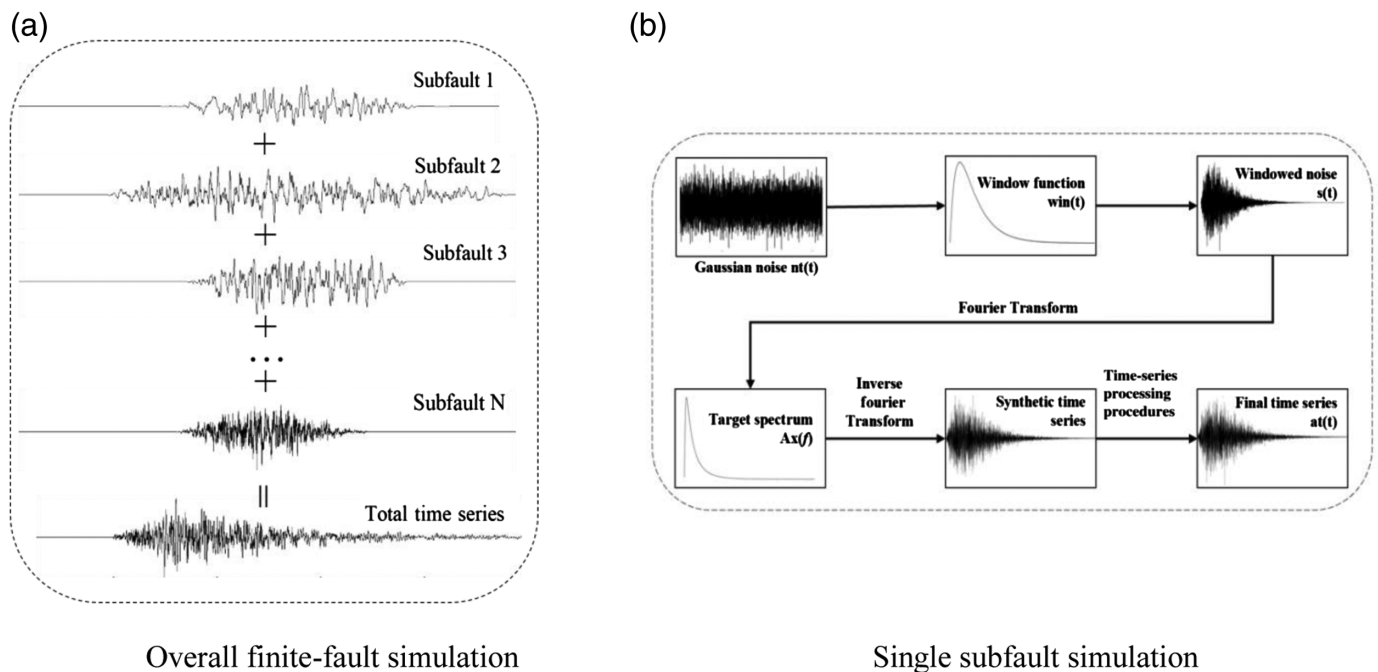
motions generated by all subfault sources in the time domain by considering proper delays of subfaults due to rupture propagation (Beresnev and Atkinson, 1997; Atkinson and Assatourians, 2015). However, there are some problems with using FINSIM for practical applications: the simulated spectral amplitude in FINSIM is dependent on the size of subfaults, each subfault is assumed to be activated more than once during the simulating procedure, and so on. In 2005, an updated open-source program named EXSIM (EXtended SIMulation) was proposed by Motazedian and Atkinson (2005). EXSIM eliminates the dependence of the spectral amplitude on the subfault size at high frequencies by introducing a scaling factor (H_{ij}) and controls the spectral amplitude at lower frequencies by a parameter defining the pulsing percentage of the rupture area.

Nevertheless, in EXSIM, the effect of the subfault size on the Fourier amplitude is not fully removed because of the incoherent summation of the ground motions generated by each subfault (Boore, 2009). Boore (2009) made some revisions on EXSIM to make it more consistent with SMSIM (a program for stochastic point source ground motion simulation, Boore, 2003), including

1. School of Civil Engineering, Guangzhou University, Guangzhou, China,  <https://orcid.org/0000-0001-6196-598X> (YT); 2. PSE Division, King Abdullah University of Science and Technology, Thuwal, Saudi Arabia

*Corresponding author: tangyuxiang56@gmail.com

© Seismological Society of America



scaling spectral amplitudes at high frequencies, removing the influences of subfault size at low frequencies, and revising the value of the stress parameter used in EXSIM (the revised EXSIM by Boore, 2009, is named as EXSIM_DMB). Atkinson and Assatourians (2015) incorporated the revisions proposed in Boore (2009) into EXSIM (they named the new version of EXSIM as EXSIM12) and validated EXSIM12 on the Southern California Earthquake Center Broadband Platform (SCEC BBP; Maechling *et al.*, 2015). They proved that EXSIM12 is able to generate similar ground motions with other broadband simulation methods contained in BBP for California, Japan, and ENA conditions.

However, there are still some fundamental problems with using the currently distributed EXSIM, including EXSIM12 (Atkinson and Assatourians, 2015), and EXSIM_DMB (Boore, 2009) (for convenience, the term EXSIM is used in this study). First, the corner-frequency model used in EXSIM is not slip correlated, and the influence of rupture velocity on the corner frequency is therefore neglected (Tang, 2022). Second, the empirical scaling relationships used in EXSIM may contain considerable uncertainties, such as the magnitude-dependent rupture scaling relationship proposed by Wells and Coppersmith (1994). Third, the current EXSIM is programmed in Fortran and is not convenient for use in engineering practices because it is difficult to follow the execution process and modify the embodied functions in the program.

Based on the abovementioned background, this article aims to introduce an enhanced software program, namely Ground-Motion Simulation System version 2.0 (GMSS2.0), written in MATLAB (see Data and Resources) and Python, for implementing stochastic finite-fault ground-motion simulations. Compared with currently distributed EXSIM, GMSS2.0 is superior in several

Figure 1. The basic principle of stochastic finite-fault ground-motion simulation: Each subfault is regarded as a point source, and the final time series is the summation of the time series of all subfaults, with proper time delays from the source and path. (a) Overall finite-fault simulation and (b) single subfault simulation.

aspects: (1) GMSS2.0 provides two different models of corner frequency and source duration (also known as rise time), one of which is rupture velocity dependent (refer to the companion article, Tang, 2022); (2) GMSS2.0 incorporates four different scaling relationships of fault size for different target regions (Wells and Coppersmith, 1994; Leonard, 2010; Kumar *et al.*, 2017; Cheng *et al.*, 2019), including relationships specific for mainland China (Cheng *et al.*, 2019), subduction interface (Kumar *et al.*, 2017), and stable continental region (SCR; Leonard, 2010); (3) GMSS2.0 provides five choices of time-series processing procedures, mainly for the baseline corrections, including the filtering approach and the empirical piecewise approach (Graizer, 1979; Chiu, 1997; Boore, 2005; Jiang, 2010; Papazafeiropoulos and Plevris, 2018); (4) GMSS2.0 incorporates two models for constructing the shear-wave velocity profile, which can be used to compute the frequency-dependent crustal amplification factors (Tang *et al.*, 2020, 2021); and (5) GMSS2.0 increases the computing speed significantly by utilizing the parallel computing toolbox contained in MATLAB.

Principle of GMSS2.0

The basic principle of GMSS2.0 is illustrated in Figure 1.

Detailed procedures for point source ground-motion simulation (principle of GMSS1.0) are clearly stated in Tang *et al.* (2021). The principles of the GMSS2.0 components are provided in the following subsections.

Fourier amplitude spectrum

According to the basic idea of finite-fault simulation, the Fourier amplitude spectrum (FAS) of acceleration for a sub-fault is expressed by

$$FA_{ij} = E_{ij} \times G_{ij} \times Ae_{ij} \times Am \times An, \quad (1)$$

in which FA_{ij} is FAS of acceleration of the ij th subfault; E_{ij} is the source component model; G_{ij} represents the geometric spreading model at a distance R_{ij} ; Ae_{ij} is the whole path anelastic-attenuation model; and Am and An are the site amplification and diminishing model, respectively. Detailed expressions for each component are given by equations (2) to (12).

The source model is expressed by:

$$E_{ij} = (2\pi f)^2 \frac{CM_{0ij}}{1 + (f/f_{0ij})^2} S_{ij}, \quad (2)$$

in which f is the frequency, C is the midcrust scaling factor; and M_{0ij} , f_{0ij} , and S_{ij} are seismic moment, corner frequency, and scaling factor for the ij th subfault, respectively.

In equation (2), C is defined by equation (3) (Atkinson, 1993):

$$C = \frac{R_p F V}{4\pi\rho_0\beta_0^3 R_0}, \quad (3)$$

in which $R_0 = 1$ km; R_p is the radiation pattern factor ($= 0.55$), usually averaged over a suitable range of azimuths and take-off angles; F is the free surface amplification factor ($= 2.0$), with the value of 2.0 strictly speaking being only valid for shear waves; V represents the partitioning factor of total shear-wave energy into two horizontal components ($= 1/\sqrt{2}$); and ρ_0 and β_0 are the density and shear-wave velocity in the vicinity of the source in g/cm^3 and km/s , respectively.

In equation (2), M_{0ij} is determined using

$$M_{0ij} = \frac{M_0 W_{ij}}{\sum_{l=1}^{nl} \sum_{w=1}^{nw} W_{lw}}, \quad (4)$$

in which M_0 is the total seismic magnitude; W_{ij} is the relative slip weight of the ij th subfault; and nl and nw are the number of subfaults along strike and down dip of the finite fault, respectively.

In equation (2), f_{0ij} is defined by Tang (2022):

$$f_{0ij} = 4.9 \times 10^6 \beta_0 \left(\frac{\Delta\sigma}{p \times M_0} \right)^{1/3}, \quad (5a)$$

$$f_{0ij} = 4.2 \times 10^6 \gamma z \beta_0 \left(\frac{\Delta\sigma}{p \times M_0} \right)^{1/3}. \quad (5b)$$

Equation (5a) is the rupture velocity-independent corner-frequency model, and it is used by currently distributed

EXSIM, whereas equation (5b) is the rupture velocity-dependent corner-frequency model, with the detailed derivation procedures of this model found in the companion article (Tang, 2022); γ in equation (5b) represents the ratio of rupture velocity (V_{rup}) and source shear-wave velocity (β_0), and z is the parameter defining the strength of high-frequency radiation. In equations (5a) and (5b), p is the parameter defining the pulsing percentage, and it is determined by equation (6):

$$p = \begin{cases} N_R/N, & N_R < N \times pp \\ pp, & N_R \geq N \times pp \end{cases}, \quad (6)$$

in which N_R is the cumulative number of pulsing subfaults, which is determined by a parameter that gives the percentage of total rupture area (pp), and N is the total number of subfaults.

In equation (2), S_{ij} is the scaling factor introduced by Boore (2009); it is used to eliminate the influences of subfault size on spectral amplitude at lower frequencies due to the incoherent summation, and it is calculated by:

$$S_{ij} = CS_{ij} \frac{1 + (f/f_{0ij})^2}{1 + (f/f_{0effij})^2}, \quad (7a)$$

in which

$$CS_{ij} = \sqrt{N}/H_{ij}, \quad (7b)$$

$$f_{0effij} = f_{0ij} / \sqrt{CS_{ij}}. \quad (7c)$$

In equations (7a), (7b), and (7c), if $f \rightarrow 0$, $S_{ij} \rightarrow CS_{ij}$, and if $f \rightarrow \infty$, $S_{ij} \rightarrow 1$.

H_{ij} in equation (7b) is the scaling factor used to eliminate subfault size influences on Fourier amplitude at high frequencies. The updated H_{ij} based on acceleration (rather than velocity) is expressed by equation (8a), and the simplified H_{ij} is expressed by equation (8b) (Boore, 2009):

$$H_{ij} = (M_0/M_{0ij}) \times \sqrt{\sum \left(\frac{f_0^2 f}{f_0^2 + f^2} \right)^2 / N \sum \left(\frac{f_{0ij}^2 f}{f_{0ij}^2 + f^2} \right)^2}, \quad (8a)$$

$$H_{ij} = \sqrt{N} \left(\frac{f_0}{f_{0ij}} \right)^2, \quad (8b)$$

in which f_0 is the corner frequency for the whole fault, which is determined by:

$$f_0 = 4.9 \times 10^6 \beta_0 \left(\frac{\Delta\sigma}{M_0} \right)^{1/3}, \quad (9a)$$

TABLE 1

Rupture Scaling Relationships Used in Ground-Motion Simulation System Version 2.0 (GMSS2.0)

Relationship	WC94	L10	K17	C19
Normal	FL = $10^{-1.88+0.50M}$ FW = $10^{-1.14+0.35M}$	FL = $10^{-2.54+0.60M}$ FW = $10^{-1.46+0.40M}$	FL = $10^{-1.722+0.485M}$ FW = $10^{-0.829+0.323M}$	FL = $10^{-4.02+0.83M}$ FW = $10^{-2.13+0.51M}$
Reverse	FL = $10^{-2.42+0.58M}$ FW = $10^{-1.61+0.41M}$	FL = $10^{-2.54+0.60M}$ FW = $10^{-1.46+0.40M}$	FL = $10^{-2.693+0.614M}$ FW = $10^{-1.669+0.435M}$	FL = $10^{-3.27+0.72M}$ FW = $10^{-1.67+0.44M}$
Strike slip	FL = $10^{-2.57+0.62M}$ FW = $10^{-0.76+0.27M}$	FL = $10^{-2.50+0.60M}$ FW = $10^{-1.49+0.40M}$	FL = $10^{-2.943+0.681M}$ FW = $10^{-0.543+0.261M}$	FL = $10^{-2.45+0.61M}$ FW = $10^{-1.38+0.41M}$
Undefined	FL = $10^{-2.44+0.59M}$ FW = $10^{-1.01+0.32M}$	*FL = $10^{-2.59+0.60M}$ *FW = $10^{-1.60+0.40M}$	†FL = $10^{-2.412+0.583M}$ †FW = $10^{-0.88+0.366M}$	FL = $10^{-2.67+0.63M}$ FW = $10^{-1.38+0.40M}$

FL and FW are the fault length and width, respectively; M is the moment magnitude; FW in L10 is obtained using the correlation between fault area and FL, assuming the fault is rectangular; and FW in C19 is obtained using the correlation between FL and FW. The unit for FL and FW is kilometers in this study. WC94 (Wells and Coppersmith, 1994); L10 (Leonard, 2010); K17 (Kumar et al., 2017); and C19 (Cheng et al., 2019).

*This scaling relationship is specifically for stable continental region.

†This scaling relationship is specifically for subduction interface.

$$f_0 = 4.2 \times 10^6 \gamma z \beta_0 \left(\frac{\Delta \sigma}{M_0} \right)^{1/3} \quad (9b)$$

G_{ij} in equation (1) is given by the subfault distance and mainly accounts for the regional geometric attenuation pattern of the seismic wave along the path. G_{ij} does not have a fixed functional format and is a region-dependent parameter.

Ae_{ij} in equation (1) is expressed by:

$$Ae_{ij} = \exp\left(\frac{-\pi f R_{ij}}{Q \beta_0}\right), \quad (10)$$

in which Q is the regional quality factor and is inversely related to anelastic attenuation.

Am and An in equation (1) are calculated by equations (11) and (12), respectively:

$$Am = \sqrt{\frac{\rho_0 \beta_0}{\bar{\rho}_z \bar{\beta}_z}}, \quad (11)$$

in which $\bar{\rho}_z$ and $\bar{\beta}_z$ are the time-averaged density and shear-wave velocity over a depth corresponding to a quarter-wave-length, respectively.

$$An = \exp(-\pi \kappa_0 f), \quad (12)$$

in which κ_0 represents the spectral decay slope at high frequencies.

The final time series of the whole fault source is computed using:

$$A(t) = \sum_{i=1}^{nl} \sum_{j=1}^{nw} H_{ij} \times Y_{ij}(t + \Delta t_{ij} + \Delta T_{ij}), \quad (13)$$

in which $A(t)$ is the total time series of the seismic signal at a site; $Y_{ij}(t)$ is the signal of the ij th subfault, which is obtained from the inverse Fourier transform of FA_{ij} shown in equation (1); Δt_{ij} is the delay time of the ij th subfault along the path; and ΔT_{ij} is the delay time for the ij th subsource and is proportional to the source duration of the subfault (T_{0ij}).

Rupture scaling relationships

Magnitude–rupture scaling relationships are important for determining the fault size and site–rupture distances in the ground-motion simulations if detailed information of fault rupture is not available. The relationship proposed by Wells and Coppersmith (1994) is universally used in the current EXSIM for all conditions. However, this relationship may introduce some uncertainties in engineering practices. More data have become available during the past decades, allowing more regionally specific scaling relationships to be developed (e.g., Leonard, 2010; Kumar et al., 2017; Cheng et al., 2019). GMSS2.0 provides four relationships for use in the source rupture modeling: (1) WC94 (Wells and Coppersmith, 1994); (2) L10 (Leonard, 2010); (3) K17 (Kumar et al., 2017); and (4) C19 (Cheng et al., 2019). WC94 is empirically developed for global use, for the data used for regression were collected from worldwide; L10 is a semitheoretical self-consistent relationship that can be used for dip-slip faults, strike-slip faults, and faults in SCRs; K17 is a new empirical scaling law that can be used for determining the rupture width, length, area, and average slip for various faulting styles, including subduction interface; and C19 is an empirical relationship typically developed for mainland China using a dataset containing 91 earthquake faults. The detailed formulas for each relationship are given in Table 1.

Figure 2 illustrates the relative scale of the four relationships for $M = 7.0$ for different fault types. Figure 2 shows that different scaling relationships impact the fault size significantly. Users may choose the most suitable one for a specific purpose.

Baseline correction

Baseline correction is required to solve the problem of unphysical shifts in the velocity and displacement traces in ground-motion simulations, and the shifts may be caused by low-frequency noise, the small initial values for acceleration and velocity, simulated ground rotation and tilting, and so on. The baseline correction approaches for recorded digital and simulated accelerometers can be classified into two types: the filtering approach removing low-frequency errors (Trifunac, 1971; Chiu, 1997; Boore, 2005) and the empirical piecewise correction approach based on velocity seismogram (Iwan *et al.*, 1985; Boore, 2001; Wang *et al.*, 2011). The filtering approach is straightforward and quite simple to use. Usually, users need to add the zero time pads into the traces and select a predetermined cutoff frequency (Boore, 2005). The criticisms of this approach are that the high-pass filter would possibly remove the important information at long periods (e.g., the permanent static drift) and it is difficult to select the “accurate” cutoff frequency (Lin *et al.*, 2018). By contrast, the empirical piecewise approach is more complicated, and users need to find several time points in the original traces. This approach is widely used to find the permanent ground displacement, which can be compared with the coseismic drifts from geodetic data such as Global Positioning System measurements and Interferometric Synthetic Aperture Radar data (Wang *et al.*, 2011). However, this approach is not convenient to use, and users may need to perform several iterations to obtain satisfactory results for strong near-field ground motions (Jiang, 2010). In this study, GMSS2.0 provides five different baseline correction methods, including the filtering approach and the empirical piecewise approach. Users may choose a suitable one for a specific purpose. The basic information of the selected methods is listed in Table 2.

Figure 3 illustrates the baseline correction effects of the five selected methods for the same randomly simulated acceleration seismogram by GMSS2.0.

Comparison with EXSIM

Because GMSS2.0 and EXSIM share the same mission, namely for generating stochastic ground-motion seismograms using finite-fault sources, it is meaningful to make a thorough comparison between the two programs. The latest version of EXSIM_DMB is used in this study (updated on 24 May 2021 by David Boore, see Data and Resources).

The input parameters for GMSS2.0 and EXSIM are listed in Table 3. The fault map and eight randomly selected sites are shown in Figure 4.

The peak ground acceleration (PGA), peak ground velocity (PGV), and Arias intensity (I_A) values simulated by GMSS2.0 and EXSIM are shown in Figure 5 for the eight selected sites, and the FAS and pseudo-acceleration response spectrum (PSA) for the eight selected sites are shown in Figure 6. As an additional comparison for varying fault size (using the magnitude-dependent scaling law proposed by Wells and Coppersmiths, 1994), the FAS and PSA for five different magnitudes for site 1 are shown in Figure 7.

Figures 5–7 show that the simulations obtained from GMSS2.0 can match those from EXSIM remarkably well. The differences for the Fourier amplitude spectra and response spectra shown in Figures 6 and 7 may come from two possible sources: (1) the difference in computing the distance in GMSS2.0 and EXSIM (i.e., GMSS2.0 regards Earth as a perfect sphere and the distance estimates may contain some uncertainties, whereas EXSIM uses an interpolation approach to get more accurate distance estimates from latitude and longitude) and (2) the difference in time domain processing techniques (e.g., the baseline correction approaches and the response spectra computation methods are different in GMSS2.0 and EXSIM). Nevertheless, the less than 5% average relative differences (with an average value of 2.53%) between GMSS2.0 and EXSIM are acceptable in practical applications (Goulet *et al.*, 2015). Because the comparison covers the magnitude range M 4–8, rupture distance range 6.9–300.48 km, azimuth range 19.1° – 354.1° , and spectral period range 0.01–10 s, the author concludes that GMSS2.0 is reliable and works as well as EXSIM for generating synthetic ground motions.

Validation Using NGA-West2 GMMs for the Generic California Condition

Additional validation is conducted by comparing GMSS2.0 simulations with five Next Generation Attenuation (NGA)-West2 ground-motion models (GMMs) for the generic California condition. The NGA-West2 GMMs were derived from large datasets and have been tested and validated by numerous studies (Abrahamson *et al.*, 2014; Boore *et al.*, 2014; Campbell and Bozorgnia, 2014; Chiou and Youngs, 2014; Idriss, 2014), so it is convincing if the simulations generated by GMSS2.0 are comparable with the estimations given by these GMMs. The input parameters for defining the FAS used in GMSS2.0 are retrieved from Atkinson and Assatourians (2015), and the site amplification factor for a reference site with $V_{S30} = 500$ m/s for California is adopted from the note for the updated SCEC BBP code (see Data and Resources). The final input parameters for this study are summarized in Table 4.

The simulated ground motions by GMSS2.0 along with the estimated ones by GMMs are shown in Figures 8 and 9.

As shown in Figures 8 and 9, the GMSS2.0 simulations generally fall within the defined acceptance criteria of the five NGA-West2 GMMs (Goulet *et al.*, 2015), indicating that

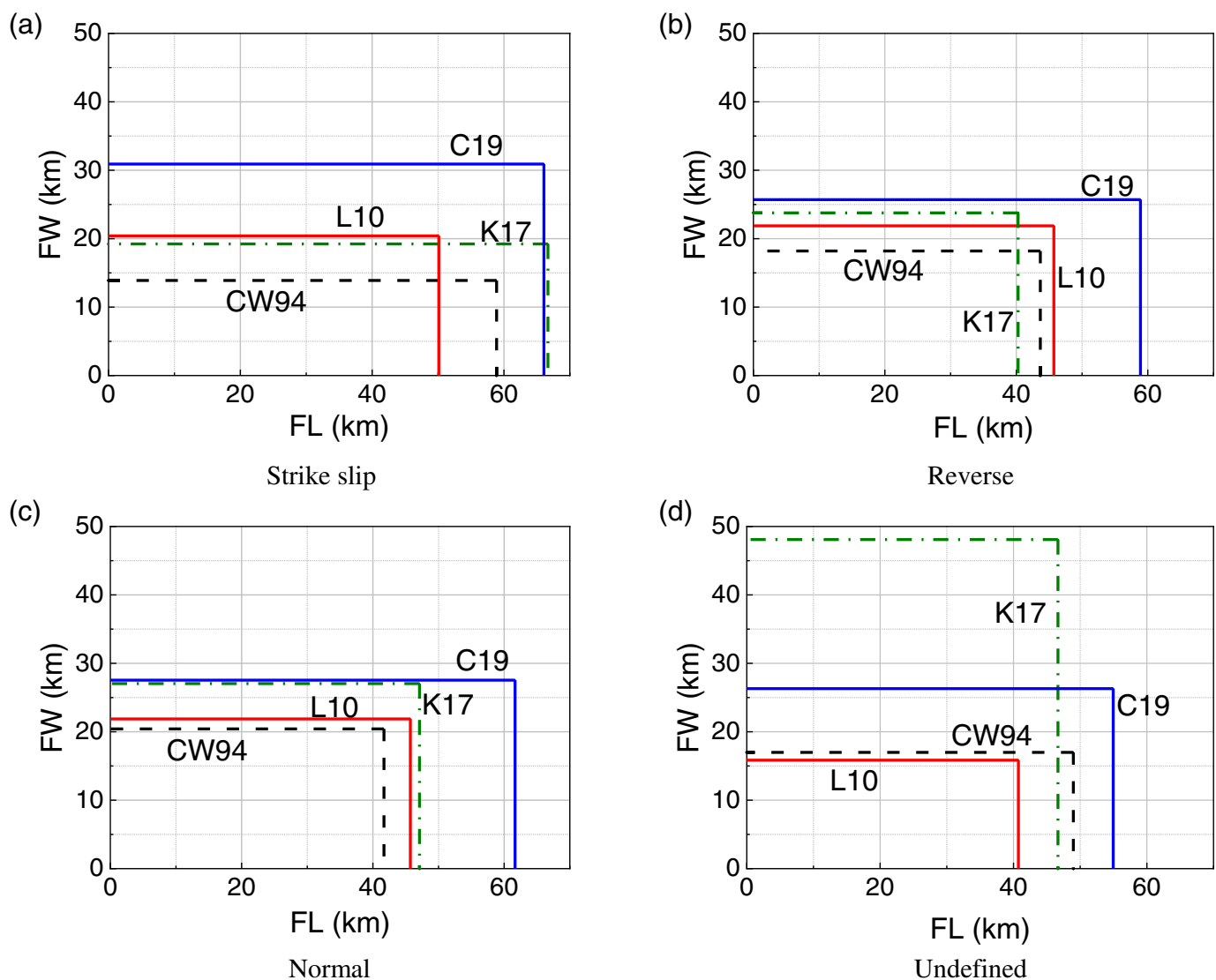


Figure 2. Illustration of four rupture scaling relationships, CW94, L10, K17, and C19, (references are listed in Table 1) used in Ground-Motion Simulation System version 2.0 (GMSS2.0) for $M = 7.0$. The Undefined for L10 and K17 indicates that these are for

stable continental region and subduction interface, respectively. (a) Strike slip; (b) Reverse; (c) Normal; (d) Undefined. The color version of this figure is available only in the electronic edition.

TABLE 2

Baseline Correction Methods Used in Ground-Motion Simulation System Version 2.0 (GMSS2.0)

Number	Method	Basic Principle	Type	References
1	G79	Use a polynomial to mimic the trend in the velocity trace and subtract the derivative of the polynomial in the original acceleration trace	Empirical piecewise	Graizer (1979)
2	C97	Use a polynomial to mimic the trend in the original acceleration trace and apply the band-pass filter to the trace additionally	Filtering	Chiu (1997)
3	B05	Apply the low-cut filter to the acceleration in the Fourier domain	Filtering	Boore (2005)
4	J10	Use a polynomial to mimic the trend in the velocity trace and subtract the derivative of the polynomial in the original acceleration trace	Empirical piecewise	Jiang (2010)
5	P18	Use a polynomial to mimic the trend in the velocity trace and subtract the derivative of the polynomial in the original acceleration trace	Empirical piecewise	Papazafeiropoulos and Plevris (2018)

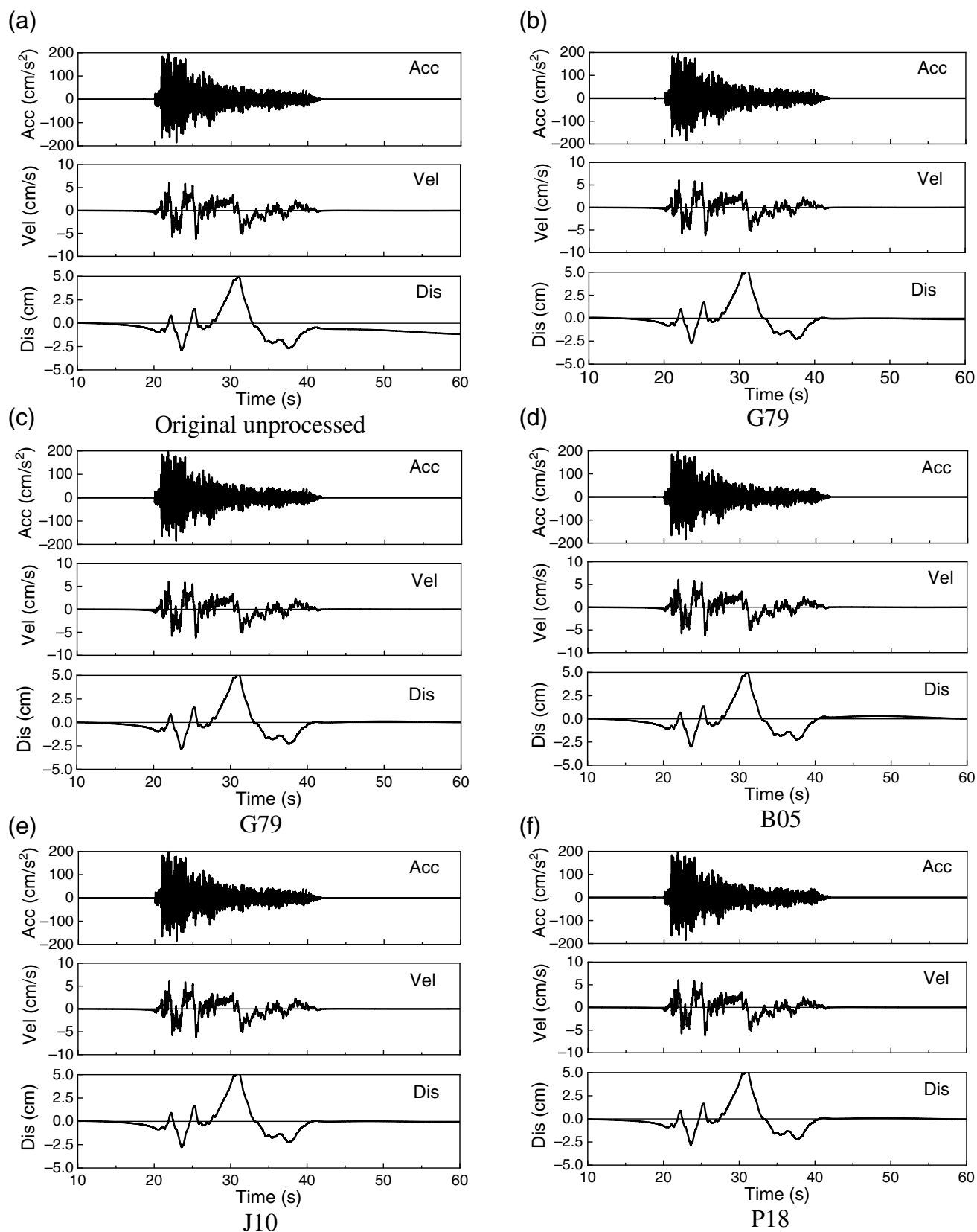


Figure 3. Illustration of the five selected baseline correction methods in GMSS2.0. The original time series is retrieved from a random simulation using $M = 7.0$ and stress drop 140 bars at a

rupture distance of 6.9 km. (a) Original unprocessed; (b) G79; (c) C97; (d) B05; (e) J10; (f) P18.

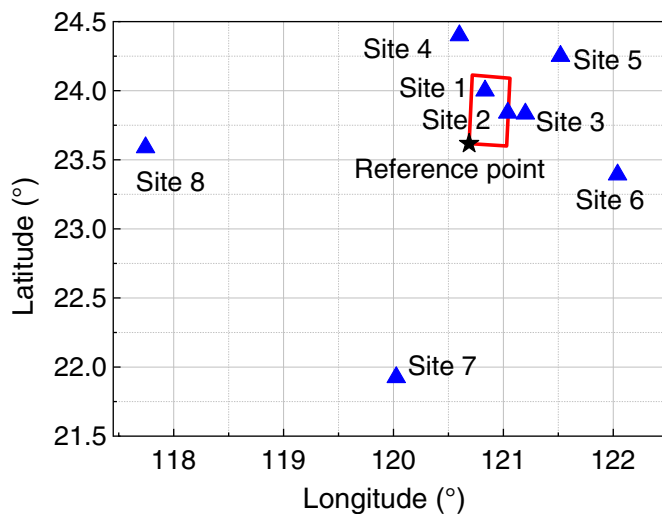


Figure 4. Fault map and distribution of the eight sites. The red rectangular is the fault, and the black star refers to the reference point. The sites are ordered based on the rupture distance given in Table 3. The color version of this figure is available only in the electronic edition.

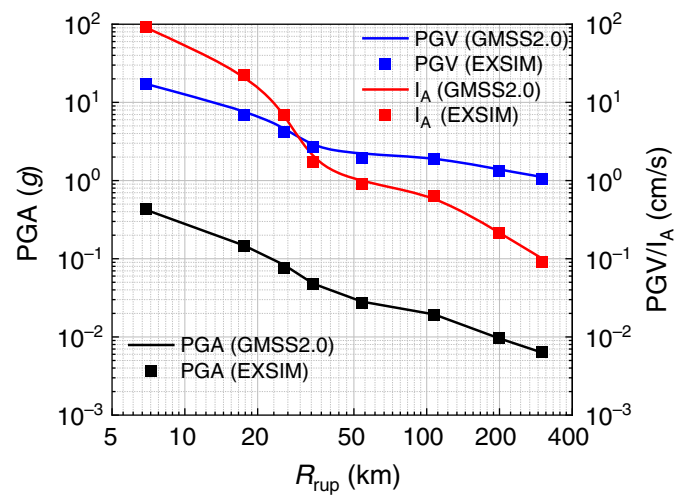


Figure 5. Simulated peak ground acceleration (PGA), peak ground velocity (PGV), and Arias intensity (I_A) by GMSS2.0 and Extended Simulation (EXSIM). The solid line is the simulation by GMSS2.0, and the square dot is the simulation by EXSIM ($M = 7.0$). The color version of this figure is available only in the electronic edition.

the GMSS2.0 simulations agree well with the GMM estimations. Figure 8 indicates that both the simulated PGA and PGV by GMSS2.0 match the value estimated by GMMs for the generic California condition, and this is because of the application of the empirical double-corner filter, which improves the goodness of fit (Atkinson and Assatourians, 2015). In particular, for M 7 and 8, the simulated PGA and PGV by GMSS2.0 are rather close to the mean estimates of the

GMMs for the entire distance range. Figure 9 specifically shows that GMSS2.0 simulations fall within the acceptance criteria of NGA GMMs at all spectral periods for the selected three scenario earthquakes at the near-distance range.

Summary and Conclusion

As an enhanced software program for implementing stochastic finite-fault ground-motion simulations, GMSS2.0 performs

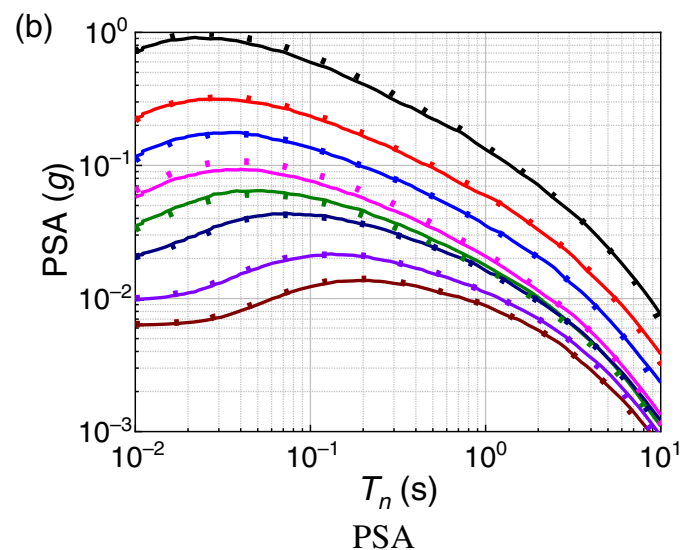
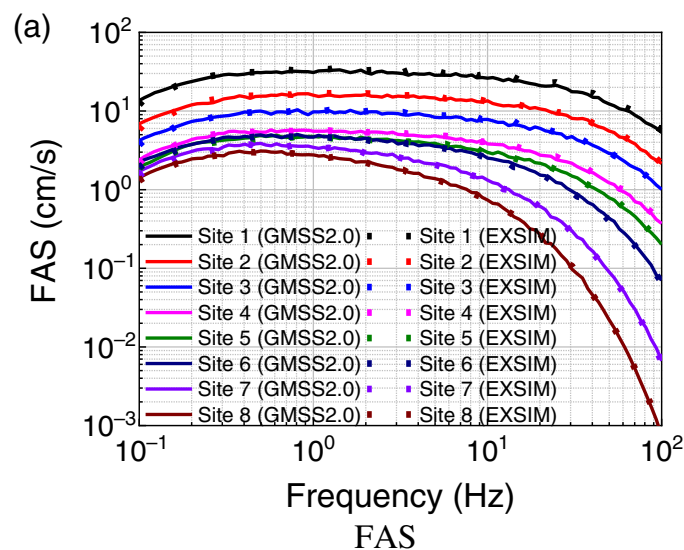


Figure 6. (a) Simulated Fourier amplitude spectrum (FAS) and (b) PSA by GMSS2.0 and EXSIM for the eight selected sites. The solid line is the simulation by GMSS2.0, and the dotted line is the

simulation by EXSIM ($M = 7.0$). The color version of this figure is available only in the electronic edition.

TABLE 3

Input Parameters for Comparing Ground-Motion Simulation System Vversion 2.0 (GMSS2.0) with EXTENDED SIMulation (EXSIM)

Parameter	Value
Time step, dt (s)	0.002
Source density, ρ_0 (g/cm ³)	2.8
Source shear wave velocity, β_0 (km/s)	3.7
Fault orientation, strike, dip (°)	3.0, 29.0
Fault dimension along strike and dip (km)	55, 40
Subfault dimension, $dl \times dw$ (km)	5×2
Location of reference point, latitude, longitude (°)	23.617, 120.689
Reference depth (km)	0.94
Moment magnitude, M_w (dyn · cm)	7.0
Stress drop, $\Delta\sigma$ (bar)	140
Reference stress drop, $\Delta\sigma$ (bar)	70
Number of simulations per hypocenter	20
Number of random hypocenters	20
Window function	Saragoni and Hart (1974), with the value of the parameter given in Boore (2009)
Corner frequency, f_0 (Hz)	Equation (9a)
High-frequency scaling factor	Equation (8b)
Rupture velocity, V_{rup} (km/s)	$\beta_0 0.8$
Slip distribution	random
Pulsing percentage (%)	50
Source duration, T_0 (s)	r/V_{rup}
Path duration	$0.05 \times R$
Geometric spreading	$R^{-1.3} (0 < R \leq 70)$ $R^{0.2} (70 < R \leq 140)$ $R^{-0.5} (140 < R)$
Quality factor	$\max(1000, 893f^{0.32})$
Crust and site amplification	1.0
κ_0 (s)	0.005
Site location, latitude, longitude (°) (rupture distance, km)	Site 1: 24.000, 120.833 (6.90) Site 2: 23.840, 121.040 (17.56) Site 3: 23.833, 121.200 (25.80)

r refers to fault radius and $r = \sqrt{dl \times dw/\pi}$.
(Continued in next column)

TABLE 3 (continued)

Input Parameters for Comparing Ground-Motion Simulation System Vversion 2.0 (GMSS2.0) with EXTENDED SIMulation (EXSIM)

Parameter	Value
	Site 4: 24.400, 120.600 (33.94)
	Site 5: 24.251, 121.520 (53.98)
	Site 6: 23.393, 122.040 (107.42)
	Site 7: 21.926, 121.026 (199.19)
	Site 8: 23.589, 117.744 (300.48)

r refers to fault radius and $r = \sqrt{dl \times dw/\pi}$.

TABLE 4

Input Parameters for Comparing Ground-Motion Simulation System Version 2.0 (GMSS2.0) with Ground-Motion Models (GMMs) for California Condition

Parameter	Value
Fault dimension along strike and dip (km)	Leonard (2010)
Subfault dimension, $dl \times dw$ (km)	2×2
Moment magnitude, M_w (dyn · cm)	6.0, 7.0, 8.0
Stress drop, $\Delta\sigma$ (bar)	150
Empirical double-corner filter	Atkinson and Silva (1997)
Corner frequency, f_0 (Hz)	Equation (9b)
High-frequency scaling factor	Equation (8b)
Source duration, T_0 (s)	$r/2V_{rup}$
Path duration	$1 + 0.18 \times R$ ($R \leq 50$) $10 + 0.05 \times (R - 50)$ ($R > 50$)
Geometric spreading	$R^{-1.0} (R \leq 40)$ $R^{-0.5} (R > 40)$
Quality factor	$\max(150, 187f^{0.55})$
Site amplification (for $V_{S30} = 500$ m/s)	0.00 Hz 1.45; 0.10 Hz 1.45 0.24 Hz 1.87; 0.45 Hz 2.17 0.79 Hz 2.48; 1.38 Hz 2.91 1.93 Hz 3.20; 2.85 Hz 3.36 4.03 Hz 3.35; 6.34 Hz 3.13 12.5 Hz 2.95; 21.2 Hz 2.99 33.4 Hz 3.11; 82.0 Hz 3.23
κ_0 (s)	0.04
Other parameters	Listed in Table 3

r refers to fault radius and $r = \sqrt{dl \times dw/\pi}$.

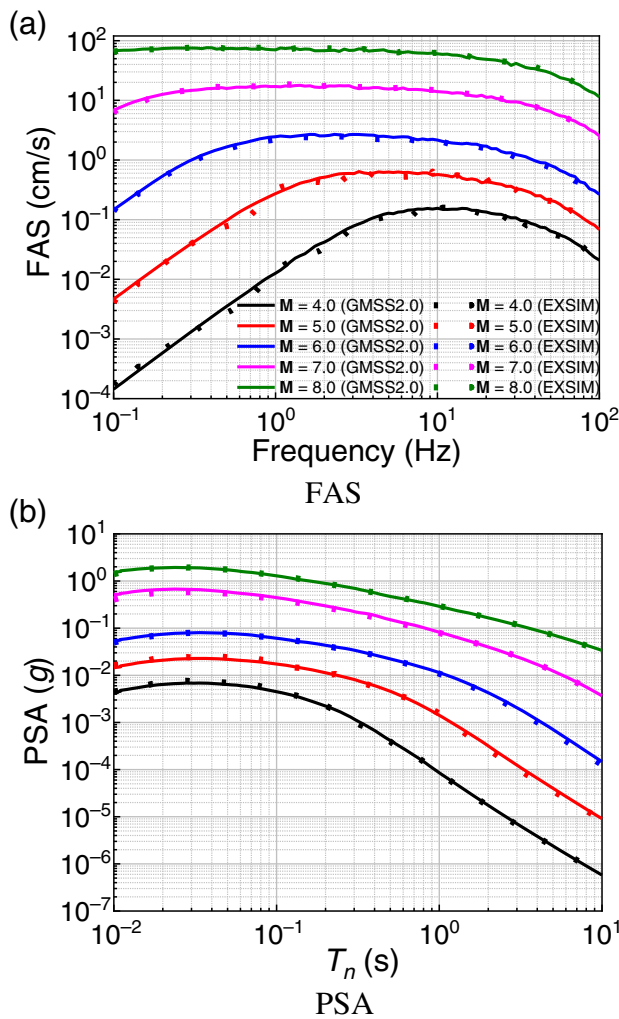


Figure 7. (a) Simulated FAS and (b) PSA by GMSS2.0 and EXSIM for M 4–8, for site 1. WC94 (Wells and Coppersmith, 1994) is adopted to determine the fault size. The solid line is the simulation by GMSS2.0, and the dotted line is the simulation by EXSIM. The color version of this figure is available only in the electronic edition.

remarkably well in generating ground motions for various geological settings over large ranges of magnitude, distances, and spectral periods. A key advantage of GMSS2.0 is that it incorporates the updated model of corner frequency and source duration, which makes the source model more theoretically consistent. In addition, it is much more flexible and convenient for end users to define the input parameters in GMSS2.0, including the rupture scaling relationships, baseline correction techniques, and crustal amplification models.

Data and Resources

Extended SIMulation (EXSIM12) is available at <https://www.seisimotoolbox.ca> (last accessed March 2021); EXSIM_DMB is available at <https://daveboore.com> (last assessed June 2021); and the Ground-Motion Simulation System version 2.0 (GMSS2.0) program is available

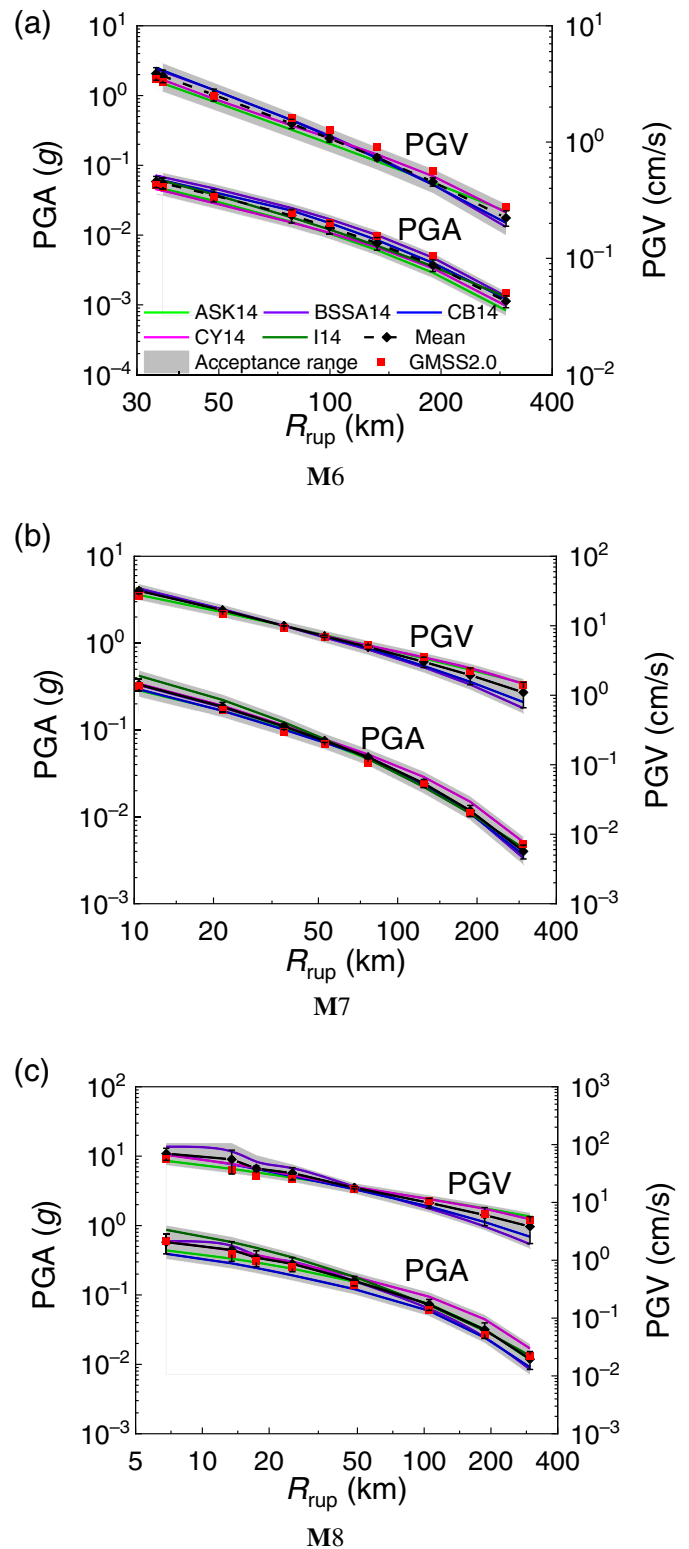


Figure 8. Comparison of PGA and PGV simulated by GMSS2.0 (the red square symbol) with those estimated by five Next Generation Attenuation (NGA)-West2 ground-motion models (GMMs). The gray shaded area indicates the acceptance criteria proposed by Goulet *et al.* (2015). (a) M 6; (b) M 7; (c) M 8. The color version of this figure is available only in the electronic edition.

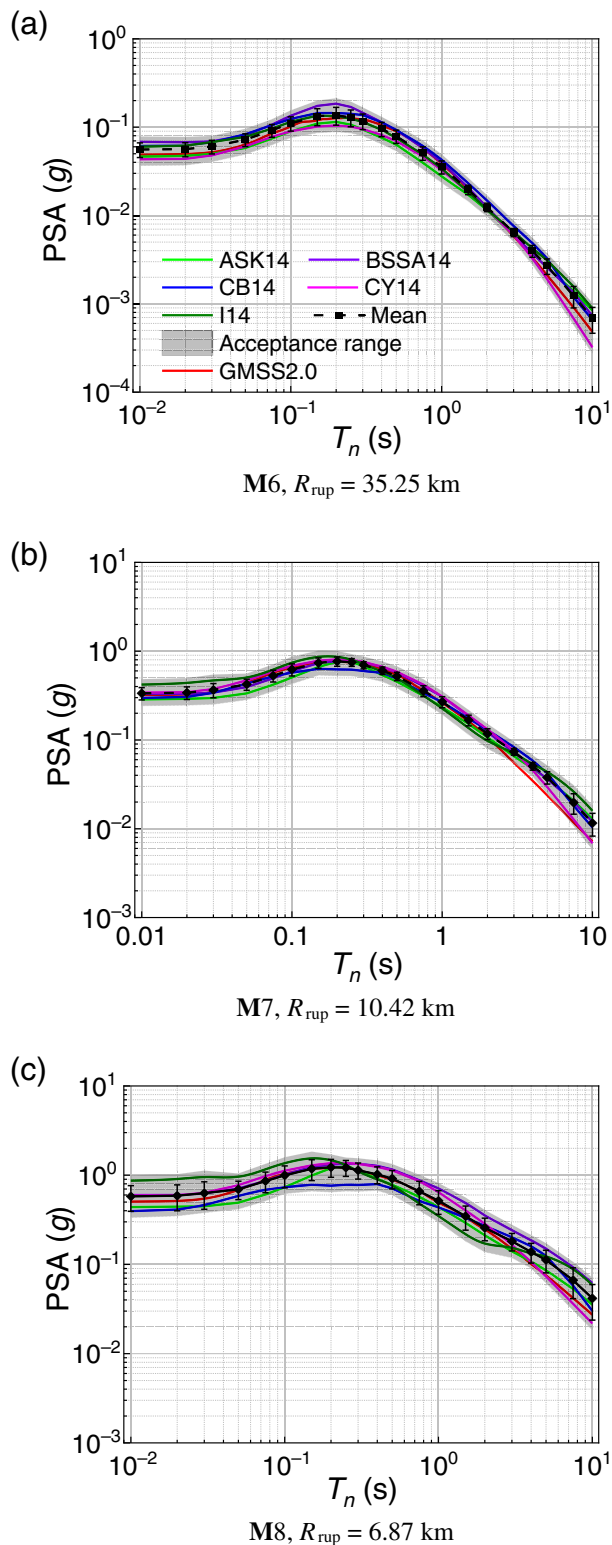


Figure 9. Comparison of PSA simulated by GMSS2.0 (the red solid line) with those estimated by five NGA-West2 GMMs for site 1 listed in Table 3. The gray shaded area indicates the acceptance criteria proposed by Goulet et al. (2015). (a) $M 6$, $R_{rup} = 35.23$ km; (b) $M 7$, $R_{rup} = 10.42$ km; (c) $M 8$, $R_{rup} = 6.87$ km. The color version of this figure is available only in the electronic edition.

at <https://github.com/Y-Tang99/GMSS2.0> (last assessed December 2021). The other relevant information to this article is available at https://daveboore.com/software_online.html (last accessed June 2021) and <https://github.com/SCECcode/bbp/tree/master/doc/pdfs> (last accessed August 2021). The MATLAB available at www.mathworks.com/products/matlab (last accessed June 2021).

Declaration of Competing Interests

The authors acknowledge that there are no conflicts of interest recorded.

Acknowledgments

The guidance and suggestions provided by David Boore for using Extended Simulation (EXSIM_DMB) are greatly appreciated. Editor-in-Chief Allison Bent is acknowledged for processing this article during the whole review procedure. In addition, the suggested comments given by the two anonymous reviewers are appreciated for improving the quality of this article. This work is supported by the Postdoctoral Office of Guangzhou City, China (Grant Number 62104343).

References

- Abrahamson, N. A., W. J. Silva, and R. Kamai (2014). Summary of the ASK14 ground motion relation for active crustal regions, *Earthq. Spectra* **30**, no. 3, 1025–1055.
- Allen, T. I. (2012). *Stochastic Ground-Motion Prediction Equations for Southeastern Australian Earthquakes Using Updated Source and Attenuation Parameters*, Geoscience Australia, Canberra, Australia, 69 pp.
- Allen, T., J. Griffin, M. Leonard, D. Clark, and H. Ghasemi (2018). *The 2018 National Seismic Hazard Assessment for Australia: Model Overview*, Geoscience Australia, Canberra, Australia, 138 pp.
- Atkinson, G. M. (1993). Earthquake source spectra in eastern North America, *Bull. Seismol. Soc. Am.* **83**, no. 6, 1778–1798.
- Atkinson, G. M., and K. Assatourians (2015). Implementation and validation of EXSIM (a stochastic finite-fault ground-motion simulation algorithm) on the SCEC broadband platform, *Seismol. Res. Lett.* **86**, no. 1, 48–60.
- Atkinson, G. M., and D. M. Boore (2006). Earthquake ground-motion prediction equations for eastern North America, *Bull. Seismol. Soc. Am.* **96**, no. 6, 2181–2205.
- Atkinson, G. M., and W. J. Silva (1997). An empirical study of earthquake source spectra for California earthquakes, *Bull. Seismol. Soc. Am.* **87**, 97–113.
- Beresnev, I. A., and G. M. Atkinson (1997). Modeling finite fault radiation from the w^n spectrum, *Bull. Seismol. Soc. Am.* **87**, 67–84.
- Beresnev, I. A., and G. M. Atkinson (1998a). Stochastic finite-fault modeling of ground motions from the 1994 Northridge, California, earthquake. I. Validation on rock sites, *Bull. Seismol. Soc. Am.* **88**, no. 6, 1392–1401.
- Beresnev, I. A., and G. M. Atkinson (1998b). FINSIM—a FORTRAN program for simulating stochastic acceleration time histories from finite faults, *Seismol. Res. Lett.* **69**, no. 1, 27–32.
- Boore, D. M. (2001). Effect of baseline corrections on displacements and response spectra for several recordings of the 1999 Chi-Chi, Taiwan, earthquake, *Bull. Seismol. Soc. Am.* **91**, 1199–1211.

- Boore, D. M. (2003). Simulation of ground motion using the stochastic method, *Pure Appl. Geophys.* **160**, 635–676.
- Boore, D. M. (2005). On pads and filters: Processing strong-motion data, *Bull. Seismol. Soc. Am.* **95**, no. 2, 745–750.
- Boore, D. M. (2009). Comparing stochastic point-source and finite-source ground-motion simulations: SMSIM and EXSIM, *Bull. Seismol. Soc. Am.* **99**, 3202–3216.
- Boore, D. M., J. P. Stewart, E. Seyhan, and G. M. Atkinson (2014). NGA-West2 equations for predicting PGA, PGV, and 5% damped PSA for shallow crustal earthquakes, *Earthq. Spectra* **30**, no. 3, 1057–1085.
- Campbell, K. W., and Y. Bozorgnia (2014). NGA-West2 ground motion model for the average horizontal components of PGA, PGV, and 5% damped linear acceleration response spectra, *Earthq. Spectra* **30**, no. 3, 1087–1115.
- Cheng, J., Y. Rong, H. Magistrale, G. Chen, and X. Xu (2019). Earthquake rupture scaling relations for mainland China, *Seismol. Res. Lett.* **91**, 248–261.
- Chiou, B. S. J., and R. R. Youngs (2014). Update of the Chiou and Youngs NGA Model for the average horizontal component of peak ground motion and response spectra, *Earthq. Spectra* **30**, no. 3, 1117–1153.
- Chiu, H.-C. (1997). Stable baseline correction of digital strong-motion data, *Bull. Seismol. Soc. Am.* **87**, 932–944.
- Goulet, C. A., N. A. Abrahamson, P. G. Somerville, and K. E. Wooddell (2015). The SCEC broadband platform validation exercise: Methodology for code validation in the context of seismic hazard analyses, *Seismol. Res. Lett.* **86**, no. 1, 17–26.
- Graizer, V. M. (1979). Determination of the true ground displacement by using strong motion records, *Izvestiya Phys. Solid Earth* **15**, 875–885.
- Idriss, I. M. (2014). An NGA-West2 empirical model for estimating the horizontal spectral values generated by shallow crustal earthquakes, *Earthq. Spectra* **30**, no. 3, 1155–1177.
- Iwan, W. D., M. A. Moser, and C.-Y. Peng (1985). Some observations on strong-motion earthquake measurement using a digital accelerograph, *Bull. Seismol. Soc. Am.* **75**, 1225–1246.
- Jiang, W. (2010). Correction method for digital strong motion acceleration records in near-field, *MSc. Thesis*, Institute of Engineering Mechanics, China Earthquake Administration, 74 pp. (in Chinese).
- Kumar, K., S. Thingbaijam, P. M. Mai, and K. Goda (2017). New empirical earthquake source-scaling laws, *Bull. Seismol. Soc. Am.* **107**, no. 5, 2225–2246.
- Leonard, M. (2010). Earthquake fault scaling: Self-consistent relating of rupture length, width, average displacement, and moment release, *Bull. Seismol. Soc. Am.* **100**, no. 5A, 1971–1988.
- Lin, Y., Z. Zong, S. Tian, and J. Lin (2018). A new baseline correction method for near-fault strong-motion records based on the target final displacement, *Soil Dynam.* **114**, 27–37.
- Maechling, P. J., F. Silva, S. Callaghan, and T. H. Jordan (2015). SCEC broadband platform: System architecture and software implementation, *Seismol. Res. Lett.* **86**, no. 1, 27–38.
- Motazedian, D., and G. M. Atkinson (2005). Stochastic finite-fault modeling based on a dynamic corner frequency, *Bull. Seismol. Soc. Am.* **95**, 995–1010.
- Papazafeiropoulos, G., and V. Plevris (2018). OpenSeismoMatlab: A new open-source software for strong ground motion data processing, *Heliyon* **4**, no. 9, e00784 1–39.
- Saragoni, G. R., and G. C. Hart (1974). Simulation of artificial earthquakes, *Earthq. Eng. Struct. Dynam.* **2**, 249–267.
- Tang, Y. (2022). An updated corner-frequency model for stochastic finite-fault ground motion simulation, *Bull. Seismol. Soc. Am.* doi: [10.1785/0120210205](https://doi.org/10.1785/0120210205).
- Tang, Y., N. T. K. Lam, and H. H. Tsang (2021). A computational tool for ground motion simulations incorporating regional crustal conditions, *Seismol. Res. Lett.* **92**, no. 2A, 1129–1140.
- Tang, Y., X. Xiang, J. Sun, and Y. Zhang (2020). A generic shear-wave velocity profiling model for use in ground motion simulations, *Geosciences* **10**, no. 10, 408, doi: [10.3390/geosciences10100408](https://doi.org/10.3390/geosciences10100408).
- Trifunac, M. D. (1971). Zero baseline correction of strong-motion accelerograms, *Bull. Seismol. Soc. Am.* **61**, 1201–1211.
- Wang, R., B. Schurr, C. Milkereit, Z. Shao, and M. Jin (2011). An improved automatic scheme for empirical baseline correction of digital strong-motion records, *Bull. Seismol. Soc. Am.* **101**, 2029–2044.
- Wells, D. L., and K. J. Coppersmith (1994). New empirical relationships among magnitude, rupture length, rupture width, rupture area, and surface displacement, *Bull. Seismol. Soc. Am.* **84**, no. 2, 974–1002.

Manuscript received 19 August 2021

Published online 16 February 2022